

# Glassy behaviour in a simple topological model

Lexie Davison\* and David Sherrington†

Dept. of Physics, Oxford University

*Theoretical Physics, 1 Keble Road, Oxford OX1 3NP, England*

September 15, 2019

## Abstract

In this article we study a simple, purely topological, cellular model which is allowed to evolve through a Glauber process. We find a non-thermodynamic transition to a glassy phase in which the energy (defined as the square of the local cell topological charge) fails to reach the equilibrium value below a critical temperature  $T_c$ , and depends strongly on cooling rate. We investigate a correlation function which exhibits aging behaviour, and follows a master curve in the stationary regime when time is rescaled by a factor of the relaxation time  $t_r$ . This master curve can be fitted by a von Schweidler law in the late  $\beta$ -relaxation regime. The relaxation times can be well-fitted at all temperatures by an offset Arrhenius law. A power law can be fitted to an intermediate temperature regime; the exponent of the power law and the von Schweidler law roughly agree with the relationship predicted by Mode-coupling Theory. By defining a suitable response function, we find that the fluctuation dissipation ratio is held until sometime later than the appearance of the plateaux; non-monotonicity of the response is observed after this ratio is broken, a feature which has been observed in other models with dynamics involving activated processes.

## 1 Introduction

Over the last few years, much work has taken place on the topic of the glass transition and the behaviour of supercooled liquids, both experimentally and through computer simulations. A great deal of this activity has involved testing the predictions of Mode-coupling Theory (MCT), which has proved thus far to reliably describe many key aspects of the dynamics of glass formers (for a review of these, see [1]). However, many questions remain, particularly with regard to the extent to which one might expect a certain system to satisfy the predictions of MCT.

The bulk of the numerical studies have taken place on binary Lennard-Jones models, hard sphere systems or amorphous silica, all of which involve a number of parameters that can be chosen to suit the study e.g. to emulate experimental systems, or to avoid crystallization etc. By contrast, the aim of this paper is to investigate a model with as few parameters as possible, in order to establish the extent to which the same features and behaviour can be reproduced. The model we use is particularly simple in that it is purely topological, involving no length scale at all. There is also the added advantage that it shows no tendency to crystallize. Whilst the model is the dual of a two-dimensional atomic model, the dynamical driving force is not the same as in that case, and there is no true phase transition.

The lack of spatial co-ordinates within the model invalidates the investigation of many familiar functions, such as the van Hove correlation function, the structure factor and the mean squared displacement. However, suitable alternatives have been identified which are, in keeping with the ethos of this paper, simpler to calculate.

---

\*ldavison@thphys.ox.ac.uk

†d.sherrington1@physics.ox.ac.uk

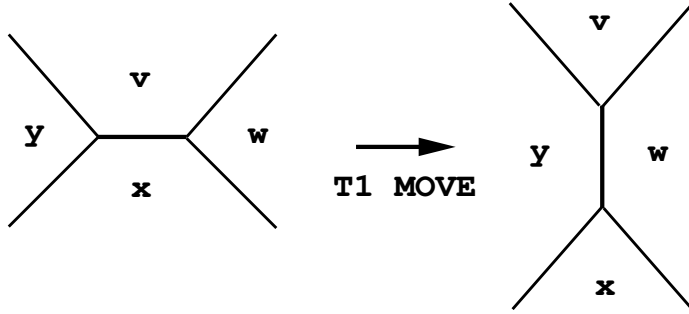


Figure 1: A T1 move: cells  $w$  and  $y$  gain a side, whilst  $v$  and  $x$  lose a side.

## 2 The Model

The model we use is that introduced by Aste and Sherrington in [2]: it is an amorphous two-dimensional tiling of cells, with 3 edges incident on a vertex and 2 cells incident on an edge. The average number of sides of the cells is constrained to be 6 by the Euler Theorem [3, 4]. These tilings are topologically stable.

If  $n_i$  is the number of sides of cell  $i$ , the topological charge  $q_i = 6 - n_i$  measures the deviation from the hexagonal configuration i.e.  $q_i$  is a measure of inhomogeneity. Topological charge is conserved under local rearrangements of the cells.

We define the energy as follows:

$$E = \sum_{i=1}^N (6 - n_i)^2 = \mu_2 N \quad (1)$$

where  $N$  is the total number of cells in the system. This quantity is naturally associated with the degree of inhomogeneity in the configuration: the ground state (a perfect hexagonal tiling) possesses zero energy.

The system is allowed to evolve through T1 moves, which are local rearrangements exchanging topological charge between four cells. Two adjacent cells lose a side each and move apart, and two second-nearest neighbours gain a side each and become nearest neighbours. The energy change associated with such a move on 4 cells  $v, w, x, y$  (as shown in Figure 1) with sides  $n_v, n_w, n_x$  and  $n_y$  is:

$$\Delta E(n_w, n_y; n_v, n_x) = 2(2 + n_w + n_y - n_v - n_x) \quad (2)$$

We use Glauber-Kawasaki dynamics, which allows evolution of the system even at zero temperature provided the move decreases the energy or leaves it unchanged. The probability  $P$  of performing a T1 move is given by:

$$P(n_w, n_y; n_v, n_x) = \frac{1}{1 + \exp(\beta \Delta E(n_w, n_y; n_v, n_x))} (1 - \delta_{n_v, 3})(1 - \delta_{n_x, 3})(1 - \delta_{w, y}) \quad (3)$$

where  $\beta$  is the inverse temperature. The first two  $\delta$ -functions forbid the production of two-sided cells, whilst the last  $\delta$ -function forbids the production of tadpoles (i.e. self-neighbouring cells); unless these forbidden formations are present at the start, they will never appear.

In the following simulations the system consists of  $N = 9900$  cells, with periodic boundary conditions. The phrase *disordered network* will be used to refer to a starting configuration obtained by randomly performing  $10^4 N$  T1 moves on a perfect hexagonal tiling. This is equivalent to running the system at  $\beta = 0$ , and results in an extremely disordered network, with a value for  $\mu_2$  of approximately 13. Time is measured in units of  $N$  attempted moves.

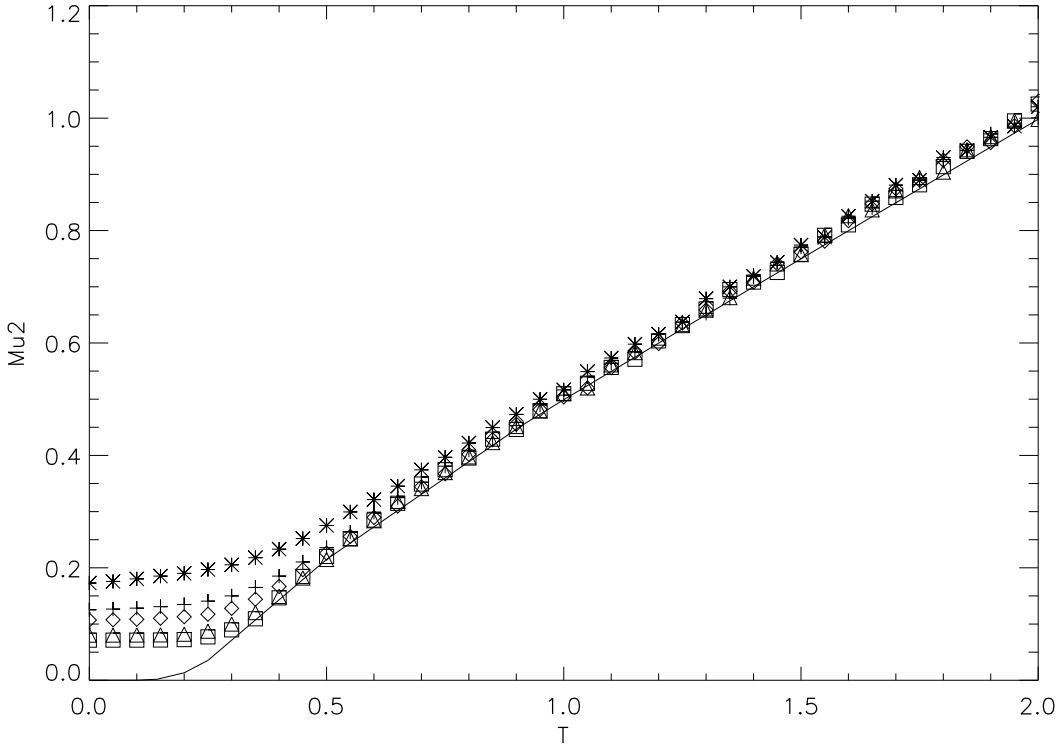


Figure 2: **The behaviour of  $\mu_2$  with temperature.** The symbols correspond to the following waiting times  $\gamma N$  at each temperature decrement of  $\delta T = 0.05$ : star -  $10N$ , cross -  $50N$ , diamond -  $100N$ , triangle -  $500N$ , square -  $1000N$ .

### 3 Relaxation Dynamics

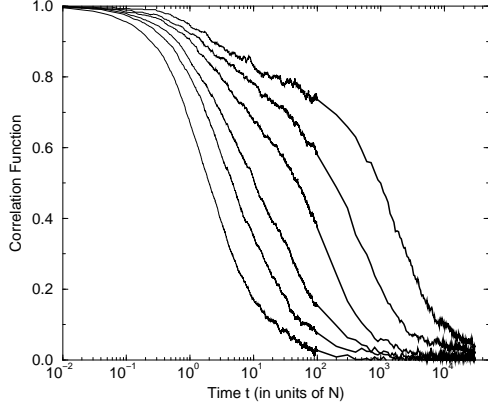
We study the temporal dependence of the energy of the system by quenching from a disordered network to  $T = 2.0$  and allowing the system to equilibrate at that temperature for  $10^4 N$  attempted moves. Cooling is then carried out by waiting a time  $t = \gamma N$  at each temperature decrement of  $\delta T = 0.05$ . The results (averaged over 3 runs) are shown in Figure 2. The solid line superimposed on the graph is the equilibrium curve: the computation of this is covered thoroughly in [2]. We can clearly see characteristic glassy behaviour: the system fails to reach equilibrium even at slow cooling rates for temperatures less than  $T \sim 0.2$ , and displays the typical strong dependence of the energy on the cooling rate, as found at low temperatures in glasses.

We also study the correlations within the system. The choice of correlation function for this particular system is by no means obvious. In previous work on this topological model, a persistence function has been studied, which measures the fraction of the total cells which have NOT been involved in a T1 move [2]. However, this provides only limited information about the system: by the very definition of the function, information about a cell is thrown away once it has been involved in a move. If the system was in a metastable state in which it performed then undid many T1 moves, this would not be revealed.

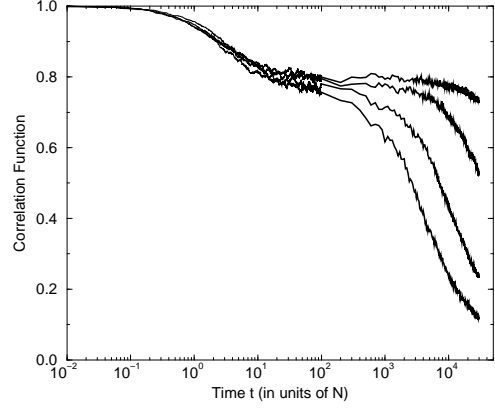
Instead we have chosen to use self-correlation functions: the first of these is

$$C(\tau, \tau + t) = \frac{\sum_{i=1}^N (n_i(\tau) - 6)(n_i(\tau + t) - 6)}{\sum_{i=1}^N (n_i(\tau) - 6)^2} \quad (4)$$

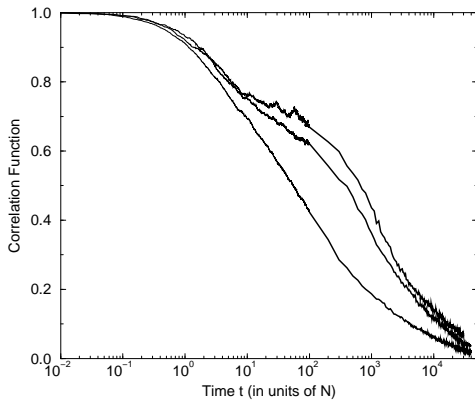
We add in passing that the results for this particular function differ negligibly in a qualitative sense from those for an energy-energy self-correlation function such as that used in conjunction with the backgammon model [5, 6].



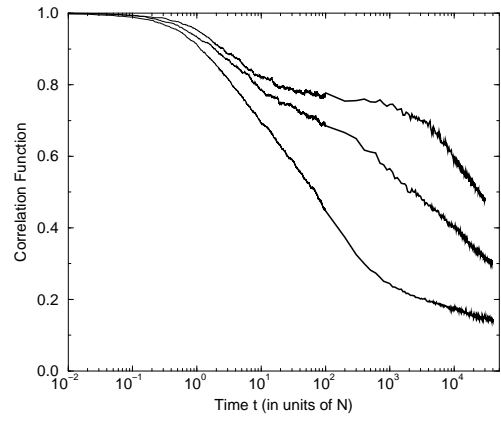
(a)  $C(t)$  for  $\beta = 1.0, 2.0, 2.5, 3.0, 3.5, 4.0$  (from left to right). These are equilibrium results.



(b)  $C(\tau, \tau + t)$  for (from left to right)  $\beta = 4.5, 5.0, 6.0, 7.0$ .  $\tau = 60,000N$ . These are non-equilibrium results.



(c)  $C(\tau, \tau + t)$  for  $\beta = 4.0$ . From left to right, the curves correspond to  $\tau = 10^2 N, 10^3 N$  and  $10^4 N$ .



(d)  $C(\tau, \tau + t)$  for  $\beta = 6.0$ . From left to right, the curves correspond to  $\tau = 10^2 N, 10^3 N$  and  $10^4 N$ .

Figure 3: Correlation functions both in and out of equilibrium (each averaged over 3 runs).

We shall first present the results in equilibrium, where the correlation functions are stationary and possess no  $\tau$  dependence. Thus the correlator  $C(\tau, \tau + t)$  becomes  $C(t)$ , a function of  $t$  only. In order to obtain stationarity, the system was allowed to equilibrate for  $60,000N$  at each temperature before measurements were taken, and for  $200,000N$  at  $\beta = 4$ . The energy was found to have equilibrated in each case and no  $\tau$  dependence was found. For  $\beta > 4$  it became impossible to achieve equilibrium within any practical timescale; even if the curves appeared stationary, the energy had not equilibrated.

Figure 3(a) shows the correlation functions for a range of temperatures. At low values of  $\beta$  (high temperatures) the correlator decays directly to zero. As the value of  $\beta$  is increased, we see a shoulder develops, indicating that two-step relaxation is taking place. If we were able to attain stationarity at higher values of beta we would see this shoulder broaden to a plateau. The plateau can be seen more clearly in Figure 3(b), which shows the correlation function for higher values of  $\beta$ , with the waiting time of  $60,000N$ ; however, one must keep in mind that this figure shows non-equilibrium results. Figures 3(c) and 3(d) show the strong  $\tau$  dependence that exists out of equilibrium.

We can study the correlation function within the stationary regime. The relaxation around the shoulder or plateau, and the early stages of the departure from it, are known as the  $\beta$ -relaxation regime. Mode-coupling Theory predicts the behaviour of conventional correlation functions in the late part of this regime (i.e. during the plateau and the departure from it) to be governed by a von Schweidler law. This states that in stationary conditions the correlator  $C(t)$  can be described as follows:

$$C(t) = f - B(t/t_r(T))^b \quad (5)$$

where  $f$  is the plateau height (also known as the non-ergodicity parameter), and both  $B$  and  $b$  are positive constants. All three should be temperature-independent, and in addition  $b$  should be independent of the choice of correlator. However, this theory is based on atoms interacting via a two-body potential and studies conventional correlation functions with explicit position dependence, such as the density-density correlator (for a recent review see [1]). Thus it is interesting to plot our rather unusual correlation function against rescaled time  $t/t_r$  to investigate the predictions of MCT in our case.

Following the procedure of Kob [7], we define the relaxation time  $t_r$  in Equation 5 as the time at which  $C(t)$  first drops below  $e^{-1}$ . Figure 4 shows the correlation functions for a range of beta against rescaled time. All the functions collapse onto a master curve in the region after the plateau or shoulder, thus obeying the time-temperature superposition principle of MCT. In the late  $\beta$ -relaxation regime this curve can be fitted by a von Schweidler law with  $f = 0.86$ ,  $B = 0.483$  and  $b = 0.42$  as shown on Figure 4. The data fits well to this law, although because of the noise the margin of error on the fitting parameters is large.

Figure 5(a) shows the relaxation time against inverse temperature. This can be fitted extremely well by the following function:

$$\tau_r = A + B \exp(C/T) \quad (6)$$

where  $A, B, C$  are constants. This is plotted on Figure 5(a), with  $A = 3.13$ ,  $B = 0.0195$  and  $C = 2.85$ . Thus at very low temperatures (high inverse temperature) the system is displaying Arrhenius behaviour, which is characteristic of strong glass formers.

In the high temperature regime, one can fit the Vogel-Fulcher law typical of fragile glass-formers i.e.  $t_r = A \exp(C/(T - T_o))$  with  $T_o = 0.202$ , but it does not suit the data as well as the offset Arrhenius curve (see Figure 5(b)).

The relaxation time is also subject to predictions by MCT, which states it should behave as:

$$t_r \propto (T - T_c)^{-\gamma} \quad (7)$$

close to the critical temperature  $T_c$ , with  $T_c$  defined through this equation. By performing such a fit on our data, we find that  $T_c = 0.218$ , as shown on Figure 5(c), with  $\gamma = 2.86$ . Neither this

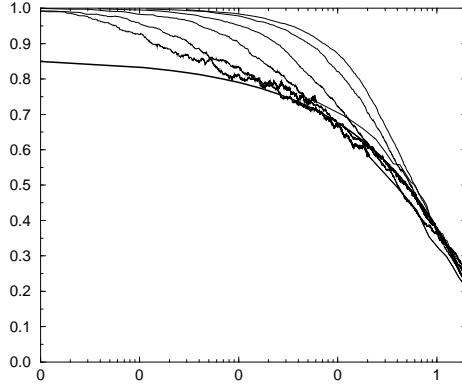


Figure 4:  $C(t)$  for  $\beta = 1.0, 2.0, 2.5, 3.0, 3.5, 4.0$  (from right to left) against rescaled time. The solid curve is a von Schweidler fit with the parameters as detailed in the text.

law nor the Vogel-Fulcher law fit the data well very close to  $T_c$ , although they both fit reasonably well slightly above  $T_c$ . However, it would seem that whilst one can fit both of these functions in certain regions, the best description at all temperatures is provided by the offset Arrhenius law.

Mode-coupling Theory predicts a relationship between the exponent  $\gamma$  in Equation 7 and the exponent  $b$  in Equation 5. They are linked by:

$$\gamma = \frac{1}{2a} + \frac{1}{2b} \quad (8)$$

where:

$$\frac{\Gamma(1+b)^2}{\Gamma(1+2b)} = \frac{\Gamma(1-a)^2}{\Gamma(1-2a)} \quad (9)$$

Using our value of  $b = 0.42$ , we find a value for  $\gamma$  of 3.12, which can be compared with the power law fit of  $\gamma = 2.86$ . These two results agree to within 10%, which is reasonable given that the noise of the data makes it is very difficult to fit either exponent accurately.

## 4 Response Functions

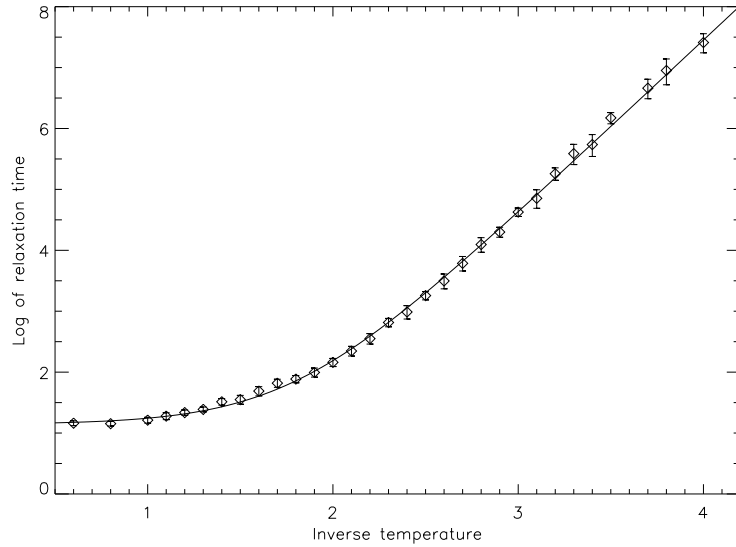
A clear indication of the presence of aging is the violation of the fluctuation-dissipation theorem [8, 9], which we shall briefly review. In equilibrium the response  $R_A$  of an observable A to an applied conjugate field relates to the appropriate time-correlation function  $C_A = \langle A(t)A(0) \rangle$  as follows (in units of  $k_B = 1$ ):

$$R_A(t) = -T^{-1} \frac{\partial C_A(t)}{\partial t} \quad (10)$$

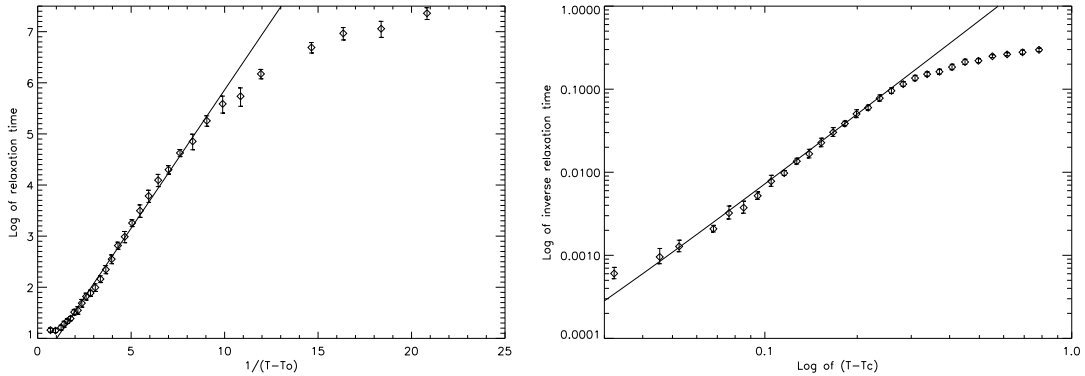
Out of equilibrium the relationship must be generalised since the correlation function is now a two-time quantity:

$$R_A(\tau, t + \tau) = -T^{-1} X_A(\tau, t + \tau) \frac{\partial C_A(\tau, t + \tau)}{\partial \tau} \quad (11)$$

with  $X_A(\tau, t + \tau)$  defined by the above equation. If  $X_A(\tau, t + \tau)$  is equal to 1, equation 11 reverts to the equilibrium case.



(a) **The logarithm of  $t_r$  against inverse temperature.** The solid curve is an offset Arrhenius fit i.e.  $\tau_r = 0.0195 \exp(2.85\beta) + 3.13$



(b) **The logarithm of  $t_r$  against  $(T - T_o)^{-1}$ .** The straight line is a best-fit Vogel-Fulcher law with  $T_o = 0.202$ .

(c) **The logarithm of the inverse relaxation time against the logarithm of  $(T - T_c)$ .** The straight line is a best-fit power law with  $T_c = 0.218$ .

Figure 5: **The behaviour of the relaxation time with temperature.**

In order to investigate autocorrelations, one can apply a field at time  $\tau$  which has a magnitude  $h_o$ , but is randomly positive or negative across the entire system. That field is left switched on, and the integrated response  $G(\tau, t + \tau)$  is measured, where:

$$G(\tau, t + \tau) = h_o \int_{\tau}^{t + \tau} R_A(t', t + \tau) dt' \quad (12)$$

For many systems it has been observed that for  $t$  and  $\tau$  both large,  $X_A(\tau, t + \tau)$  depends on  $t, \tau$  only through the correlator i.e.  $X_A(\tau, t + \tau) = x(C(\tau, t + \tau))$ . If that is indeed the case, one finds:

$$\frac{-TG(\tau, t + \tau)}{h_o} = \int_1^C x(C') dC' \quad (13)$$

Under those conditions the slope of a parametric plot of  $-TG(\tau, t + \tau)/h_o$  against the relevant correlation function is the interesting quantity, since:

$$\frac{\partial}{\partial C} \left( \frac{-TG(\tau, t + \tau)}{h_o} \right) = x(C) \quad (14)$$

One would expect to find a slope of exactly  $-1$  where the fluctuation-dissipation ratio is upheld. Where the ratio is broken, the slope gives information about the form of  $X_A(\tau, t + \tau)$ .

In our particular case, we apply a perturbation  $h_o \sum_{i=1}^N \epsilon_i (n_i - 6)$  at time  $\tau$ .  $\epsilon_i$  is randomly assigned to be  $+1$  or  $-1$ , and  $h_o$  is chosen carefully to ensure linear response whilst also obtaining a reasonable signal-to-noise ratio. We follow the integrated response  $G(\tau, t + \tau) = \sum_{i=1}^N \epsilon_i (n_i - 6)$ . It is easy to see that the appropriate correlation function for this observable is of the form of that given in equation 4, although one must be careful with normalisation factors. The data is in general very noisy and it is necessary to average over at least 8-10 different field configurations to be able to reach any conclusions.

Before presenting results, we draw attention to the unusual nature of our integrated response function. At low temperatures almost all the cells within the system are 5, 6 or 7-sided, with the vast majority being 6-sided. This means that a large proportion of the system *makes no contribution to the response whatsoever*. Furthermore, processes which reduce the energy by turning pentagons and heptagons into hexagons in fact reduce the response. This will be discussed in more detail in the following paragraphs; in the meantime, it is sufficient to remember that the integrated response function used here has some unusual features.

Figure 6 shows the results for  $\beta = 4$  and  $5$ . These are non-equilibrium results in all cases, as the waiting times are not long enough for the system to have equilibrated. The superimposed straight lines have slope  $-1$ , but are not best fits; they are there to give the eye a comparative reference. These plots should be examined from right to left i.e. short times are on the right, where  $C(\tau, \tau + t)$  is close to 1, and long times are on the left. We see that for short times the fluctuation-dissipation ratio is upheld; the slope is  $-1$  for all values of  $\tau$ , although the intercept does of course vary. In fact, the ratio is not broken until  $C(\tau, \tau + t)$  has decreased to  $\sim 0.6$ : this is considerably lower than the value of  $C(\tau, \tau + t)$  at which the plateau occurs. Thus the fluctuation-dissipation ratio is obeyed for a timescale larger than that of the onset of the plateau. After the ratio has been broken, curves for different  $\tau$  behave differently, tending towards the equilibrium straight line of slope  $-1$  as  $\tau$  increases. The non-monotonicity displayed clearly in Figure 6(a) occurs in every case, although at lower temperatures one cannot run long enough to see it, as in Figure 6(b). Non-monotonicity of the response has been noted in several other models and will be discussed briefly in the next section. In the meantime, with regards to this model this unusual behaviour can be understood if we now turn to a discussion of the processes dominating the evolution of the system.

At low temperatures, out of equilibrium, moves which increase the energy occur very rarely; we can consider the system to evolve by a combination of zero-energy moves and moves which reduce the energy. After a short time ( $\sim 10^3 N$ ) the system consists almost entirely of 5, 6 and 7-sided cells. Under these conditions the possible moves are as shown in Figure 7(a) and 7(b).

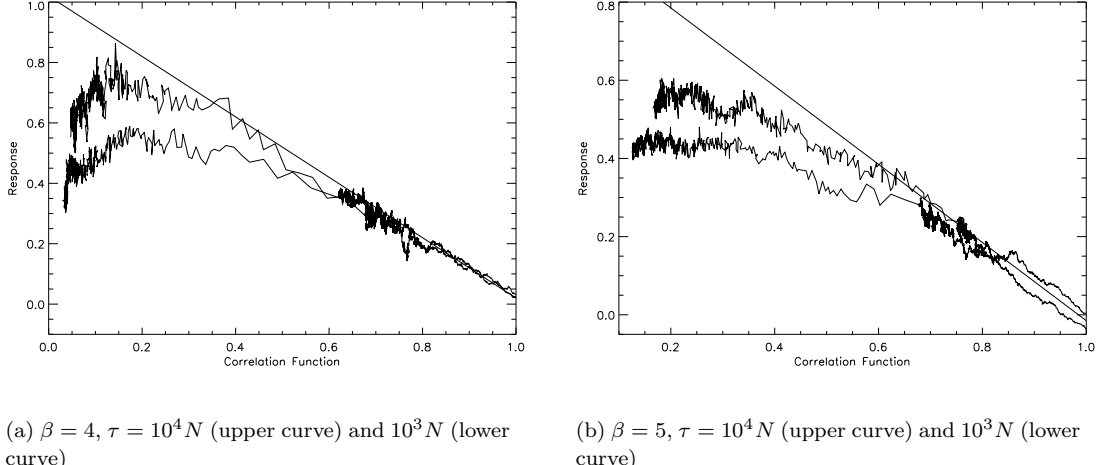


Figure 6:  $\frac{-TG(\tau, \tau+t)}{h_o}$  plotted parametrically against  $C(\tau, \tau+t)$  at different  $\beta$  and  $\tau$  (averaged over 10 runs).

The moves in Figure 7(c) are considered very unlikely due to the low probability of finding four non-hexagons clustered together; this is corroborated by the extreme rarity of finding octagons and rectangles present. We see from Figure 7(a) that in certain topological arrangements, pentagons and heptagons can effectively diffuse freely through the system; in particular, pentagons and heptagons can ‘pair up’ to move through the system together with no energy cost. To reduce the energy, one must annihilate two or more ‘defects’ (i.e. non-hexagons) as in Figure 7(b); this requires the absorption of a 5-7 pair by an isolated pentagon or hexagon, or the annihilation of two 5-7 pairs. This brings us to a conceptual picture containing both fast and slow dynamics: the fast dynamics is due to the rapid diffusion of 5-7 pairs moving freely through the system, whereas the slow dynamics is due to annihilation processes. The latter can be broken down into two different types: absorption of a 5-7 pair by either a heptagon or a pentagon (which can also rearrange the network such that isolated pentagons and heptagons become 5-7 pairs), and the complete annihilation of two 5-7 pairs. Of course, in equilibrium an equal number of 5-7 pairs are created as annihilated/absorbed, but in the relaxation to equilibrium, annihilation has the upper hand as the system starts from a configuration in which there are more 5-7 pairs present.

The effect of the field is to try and ‘pin’ defects onto the appropriate cell i.e pentagons try to settle on sites with  $\epsilon_i = +1$  and heptagons on  $\epsilon_i = -1$ . Thus with the field switched on, the diffusion processes move the defects around until they are on the appropriate sites, and in this way increase the value of the response  $-TG(\tau, \tau+t)/h_o$ . However, annihilation processes remove defects from the system entirely, thus reducing the response and also reducing  $C(\tau, \tau+t)$ . We have competition between the annihilation processes and the diffusive processes; when annihilation dominates, the slope on the parametric plot becomes positive, as seen for small values of  $C(\tau, \tau+t)$  in Figure 6(a). If one looks instead at a quantity such as  $-TG(\tau, \tau+t)/h_o\mu_2$  (in some sense a ‘response per defective cell’) one finds that the slope remains negative: this tells us that the diffusion processes are succeeding in placing more of the defects that remain on the appropriate sites, but the number of those defects present in the system is declining. The value of the response reached when the system finally achieves equilibrium depends on the waiting time  $\tau$ , and increases as  $\tau$  increases; this is because both the response and the correlation function have been normalised by a factor that is equivalent to the energy at time  $\tau$  (see equation 4).

This picture of diffusion and annihilation/creation processes is helpful to an understanding of the plateaux in the correlation functions at low temperatures. The initial descent to the plateau is due to diffusing 5-7 pairs, which quickly move the network away from the starting configuration.

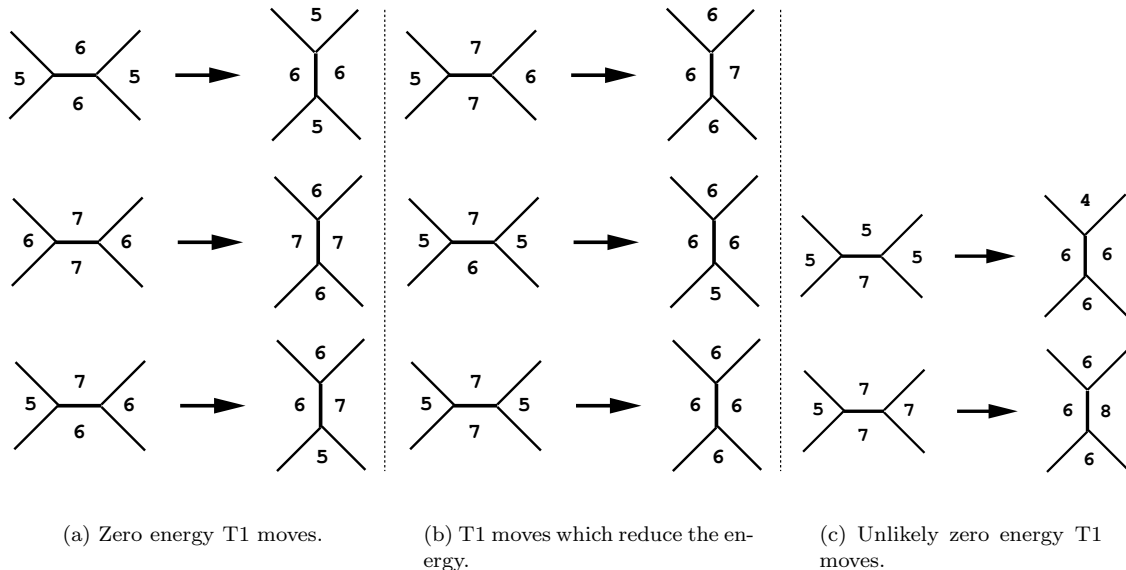


Figure 7: The possible T1 moves at low temperatures.

However, the lone defects are trapped, and can only be freed by a move which costs energy or by absorption of a 5-7 pair; both of these processes occur on a timescale which is temperature-dependent, and thus the length of the plateau itself is dependent on the temperature. This picture of trapped or caged defects is conceptually similar to that typically used when dealing with Lennard-Jones binary models [7] [10].

## 5 Concluding remarks

In summary, we have tested some of the predictions of MCT on this simple glassy model, and find that this theory can indeed be used to describe the behaviour of the system in so far as we have investigated, although this description fits some features more closely than others. The correlation function follow a von Schweidler law as predicted in the late  $\beta$ -relaxation regime, and the exponent of this roughly agrees with the exponent of the power law fitted to the relaxation time data. However, the relaxation times fit better to an offset Arrhenius law in all temperature regimes.

Investigation of the fluctuation-dissipation ratio reveals an interesting feature, namely non-monotonicity of the response. This is a feature which has also been observed in other simple models; for example, vibrated granular media [11], constrained Ising chains and the Backgammon model in one dimension [12], and also recently in a two-dimensional short-range spin model with uniform ferromagnetic 3-body interactions [13]. In each case, the dynamics at low temperatures can be considered to involve activation over energy barriers; as mentioned in [13], this raises the question as to whether this is a generic feature of models with activated dynamics.

## 6 Acknowledgements

The authors would like to thank T. Aste and J. P. Garrahan for helpful discussions, and EPSRC(UK) for financial support - DS for research grant GR/M04426, and LD for research studentship 98311155.

## References

- [1] W. Götze, J. Phys. Cond. Matt. **11**, A1 (1999).
- [2] T. Aste and D. Sherrington, J. Phys. A **32**, 7049 (1999).
- [3] D. Weaire and N. Rivier, Contemp. Physics **25**, 59 (1984).
- [4] J. Stavans, Rep. Prog. Mod. Phys. **56**, 733 (1993).
- [5] F. Ritort, Phys. Rev. Lett. **75**, 1190 (1995).
- [6] S. Franz and F. Ritort, Europhys. Lett. **31**, 507 (1995).
- [7] W. Kob, J. Phys. C **11**, R85 (1999).
- [8] J.-P. Bouchaud, L. Cugliandolo, J. Kurchan, and M. Mezard, p161 in **Spin Glasses and Random Fields**, A.P Young (Ed) (1998).
- [9] G. Parisi, Phys. Rev. Lett. **79**, 3660 (1997).
- [10] T. Gleim and W. Kob, Europhys. J. B **1**, 83 (2000).
- [11] M. Nicodemi, Phys. Rev. Lett. **82**, 3734 (1999).
- [12] A. Crisanti, F. Ritort, A. Rocco, and M. Sellitto, cond-mat/0006045 .
- [13] J. P. Garrahan and M. E. J. Newman, cond-mat/0007372 .